Hyperspectral imaging analysis of corrosion products on metals in the UV range

Aoife Keane[a], Paul Murray[a], Jaime Zabalza[a], Antonio Di Buono[b], Neil Cockbain[b], Robert Bernard[c]
[a]University of Strathclyde, 16 Richmond St, Glasgow G1 1XQ, UK;
[b]National Nuclear Laboratory, Havelock Rd, Workington CA14 3YQ, UK;
[c]Sellafield Ltd., Seascale, Cumbria, CA20 1PG, UK

ABSTRACT

This work reviews and presents a comparison of hyperspectral imaging results when analysing corrosion products in the ultraviolet (UV) range (250 nm – 500 nm), visible near-infrared (VNIR) range (400 – 1000 nm) and shortwave-infrared range (900 – 2500 nm). In related and prior work in our group, corrosion products on steel have been detected using hyperspectral imaging in the VIS, NIR and SWIR regions of the spectrum. However, an extensive review of the academic literature has revealed that the hyperspectral response of corrosion in the UV has not been reported. To address this, we present our results of imaging corrosion products on metal substrates using our Headwall UV-VIS Hyperspectral imaging sensor. These results are contrasted with the same samples imaged using our Headwall VNIR E series and Headwall SWIR 640 Hyperspectral imaging sensors. Our initial results indicate that corrosion spectra in the UV are separable from those of steel, but that the VNIR is the most appropriate range for this type of determination.

1. INTRODUCTION

Corrosion forms on steel and other metals and can lead to product loss, damaging the integrity of the material. Many methods exist for the assessment and identification of corrosion. Due to the product loss associated with corrosion it is often imperative to use non-destructive testing methods to evaluate its presence to not further jeopardise the material. Such non-destructive methods include surface profile measurements and colour photography[1], and eddy current [2]. The measurements taken with colour photography and surface profilometry boast advantages of being able to measure large surface areas at once, rather than assessing a single point. Hyperspectral imaging (HSI) similarly boasts the ability to image large areas at high spatial resolution and imaging speed. HSI benefits from combining spectral and spatial features of the imaged material. By assessing hundreds of channels for different wavelengths of electromagnetic (EM) radiation, the spectral characteristics of the material can give more detail than the three channels in colour photography. Work looking at the identification of corrosion using HSI, has previously focused on the visible (VIS), near-infrared (NIR), and shortwave-infrared (SWIR) ranges of the EM spectrum. Though the works in literature are limited, they have produced significant success. Remote sensing applications have identified the 400 – 1000 nm region as the potential important range to identify separate iron oxide phases [3]. This is consistent with the 650 – 700 nm range which gives iron corrosion products the signature rust-red hue.

In [4] the severity of corrosion was assessed based on the corrosion products present on the surface of carbon steel (s235) in the SWIR range (900 – 1700 nm) and cross-correlating retrieved spectra with the pure reference spectra for products including hematite, lepidocrocite, and goethite. The results are represented as the percentage total of each corrosion mineral present in the sample, as compared with the percentages of minerals present found by the Fourier Transform Infrared (FTIR) spectroscopy ground truth. There is no confirmation as such of whether the HSI spatial identification of a given mineral is correct. Overall using this range of the EM spectrum, the work puts forward a means to identify different corrosion products with a maximum absolute error of 36%.

In [5] the spectral aspect of HSI was exploited to remove the visual ambiguity that can be present with RGB images taken in-situ. The input data was non-corroded ASTM A572 structural steel; coated steel; and steel corroded with acids, sulphates, and salts. A VNIR HSI camera was used, with wavelengths of 397 – 1007 nm.

This is a peer-reviewed, accepted author manuscript of the following article: Keane, A., Murray, P., Zabalza, J., Di Buono, A., Cockbain, N., & Bernard, R. (2023). Hyperspectral imaging analysis of corrosion products on metals in the UV range. In N. J. Barnett, A. A. Gowen, & H. Liang (Eds.), Hyperspectral Imaging and Applications II: Proceedings Volume 12338 SPIE. https://doi.org/10.1117/12.2647429

This data is reduced using PCA, and then fed into an SVM to classify the pixels of the hyperspectral image. The analysis shows that the VNIR spectra for each class are distinguishable for a few regions, such as acid, non-corrosion, and coating between 523 – 580 nm, and sulphate and salt between 866 – 1004 nm. The SVM could reliably distinguish between non-corrosion, coated steel, and acid corrosion. There was a good deal of misclassification between salt and sulphate-induced corrosion, 13% and 18% respectively, explained by the similar chemical composition of the samples.

The thesis presented in [6] evaluated what they refer to as the UV-VIS-NIR range (450 - 850 nm wavelength interval) of the EM spectrum for corrosion samples on stainless steel. It found that HSI was sufficient to detect corrosion on these samples, but that the spectra across the range of assessed wavelengths lacked any features that would allow for iron oxide phase classification, beyond the general positive intensity gradient present at all locations where iron oxides and hydroxides are found.

Through thorough review of literature, a gap was identified in the spectral reporting of corrosion and corrosion products on steel for wavelengths shorter than 450 nm. The paper presented compares the results of HSI of corrosion on steel in the UV range with that of the results of the VNIR and SWIR range. Thus, the results put forward in this paper evaluate the usefulness of this portion of UV range in the identification of corrosion products on steel.

2. MATERIALS AND DATA ACQUISITION

The materials imaged here were three samples of 316L steel filters approximately 2 cm x 2 cm in size, with two of the filters corroded in a sodium chloride salt bath, and the remaining sample left unmarred, as seen on the left side of Figure 1. These were imaged using three Headwall Hyperspectral imaging sensors covering a range of wavelengths between 250 and 2500 nm. Figure 1a shows the UV-VIS image produced from the UV-VIS sensor which provides 440 bands of wavelengths between 250 – 500 nm; Figure 1b shows the image from the Headwall VNIR E series sensor with 373 bands between 400 – 1000 nm; and Figure 1c shows the Headwall SWIR 640 image, with 272 bands in the range of 900 – 2500 nm.

a)

b)

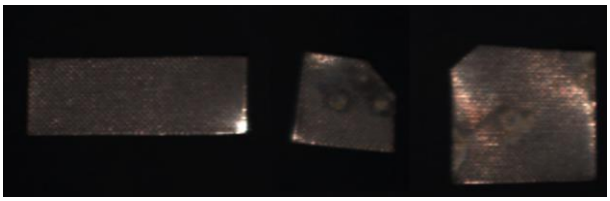

c)

Figure 1. a) UV composite image of 316L filters; b) VNIR composite image of 316L filters; c) SWIR composite image of 316L filters

The hyperspectral images of these samples were captured by placing the steel samples on a sliding stage placed 40 cm from the camera. The nature of image acquisition was a push broom system where the image is collected strip-by-strip with a line of horizontal pixels assessed across the whole spectral range at one time and then moving across to the next line of pixels. The raw hyperspectral image cube was calibrated using white and dark reference spectra, with the white reference coming from a white tile of Spectralon, and the dark reference captured by covering the lens of the camera completely using its lens cap. The calibration was done automatically using the Headwall software. The details of the setup for collecting data with each camera are detailed in Table 1.

When the UV HSI image was taken, the final band was null – every pixel value was zero. For this reason, this wavelength is excluded from the spectra assessed in this paper and the actual number of bands assessed is 439, with a range of 249.178 - 499.645 nm. Equally, the SWIR HSI image gave unusual results for the first 10 bands, so these are excluded, meaning 262 bands covering wavelengths between 949.075 - 2508.02 nm are assessed.

Table 1. Features and calibration settings of the images produced with each hyperspectral sensor.

Feature	UV	VNIR	SWIR
Illumination Source	Xenon lamp	Tungsten Halogen lamp	Tungsten Halogen lamp
Horizontal Resolution (pixels)	1280	1600	640
Exposure Time (ms)	40	30	30
Frame Period (ms)	50	40	35
Actual Spectral Range (nm)	249.178 - 499.645	398.523 – 1001.4	949.075 - 2508.02

3. DATA CONDITIONING

The original hyperspectral image of all three samples, Figure 1, was separated into three smaller images, to assess the spectral responses of corrosion for each sample as seen in Figure 2. The samples are referred to henceforth as samples A, B, and C.

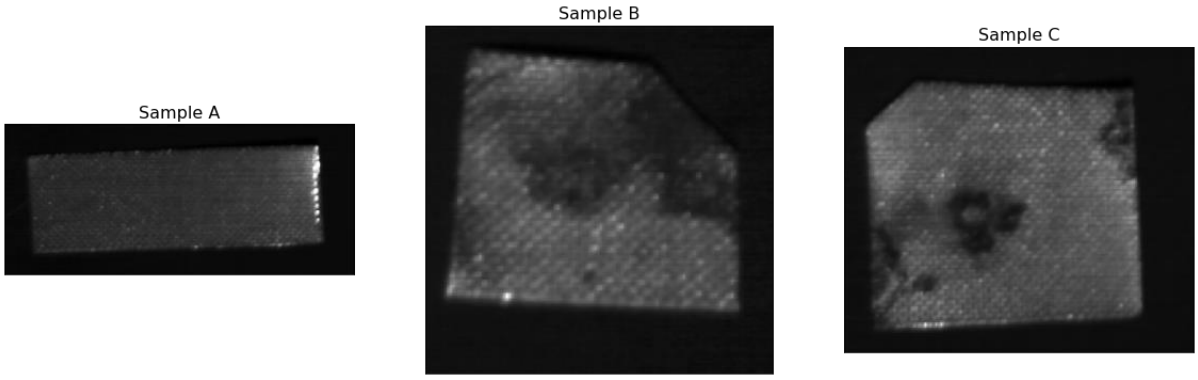

Figure 2. Example of samples separated into individual images for ease of assessment

To limit the influence of noise in the samples, a second order Butterworth filter with a cut-off at 40% of the Nyquist frequency was applied to the spectra. This removed high frequency noise whilst maintaining the lower frequency shape and features of the spectra. The effect of this filtering is demonstrated in Figure 3.

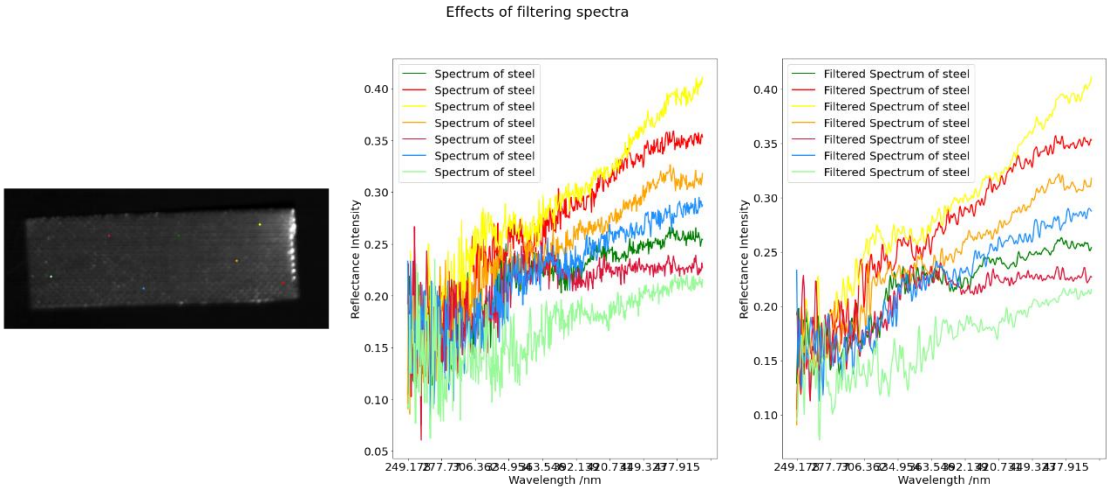

a) b) c)

Figure 3. a) UV Sample A with the pixels probed indicated on it; b) Probed unfiltered steel spectra; c) Probed filtered spectra of steel.

4. OBSERVED SPECTRAL RESPONSES

Corrosion locations were determined by using human visual inspection of the RGB image of the samples as ground truth, but as such, there lacks a definitive guarantee that the pixels being labelled as non-corroded have not undergone a chemical change that is not yet noticeable under RGB imaging. Therefore, in this work, there is no chemical ground truth; future work will address this. Ground truth values for steel are extracted from sample A, as this sample had not been exposed to the saline solution and as such can be considered a sample of purely 316L steel. An average spectrum from this sample was collected to have a baseline value for 316L steel to

compare corroded areas on other samples. Figure 4 shows these mean spectra, for each camera, when highly reflective areas were discounted.

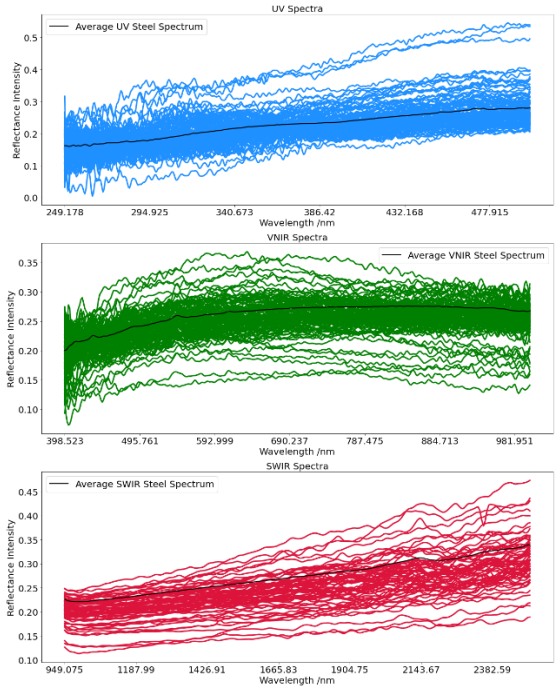

Figure 4. Average 316L spectrum (black) for UV, VNIR and SWIR cameras, and a number of sample steel spectra to demonstrate that the average fits the general shape of the data.

This shows that the individual steel spectra can vary significantly, and as such, there is a general lack of features and consistency within the steel. The average spectra, therefore, offer representations of steel in each of the spectral ranges. The pixels on the other samples were compared to the relevant average in order to highlight the separable features between the corrosion and the steel it has formed on.

Each camera was used to assess the same corroded areas on both Sample B and Sample C in order to give a fair comparison between the distinguishable spectral features.

1.1 UV Analysis (250 – 500 nm)

Figure 5 shows a number of probed corrosion pixels on sample B in the UV range, contrasted with the average steel spectrum and a random sample of uncorroded steel from the same sample. Reviewing the spectra shows that areas of corrosion have a lower reflectivity across all wavelengths than the steel. Looking specifically at sample C, Figure 6, another feature emerges: that of a double peak at 469 and 474 nm. However, as this double peak is present on the non-corroded steel samples as well, it can be disregarded as a feature of corrosion and is instead likely representative of something else.

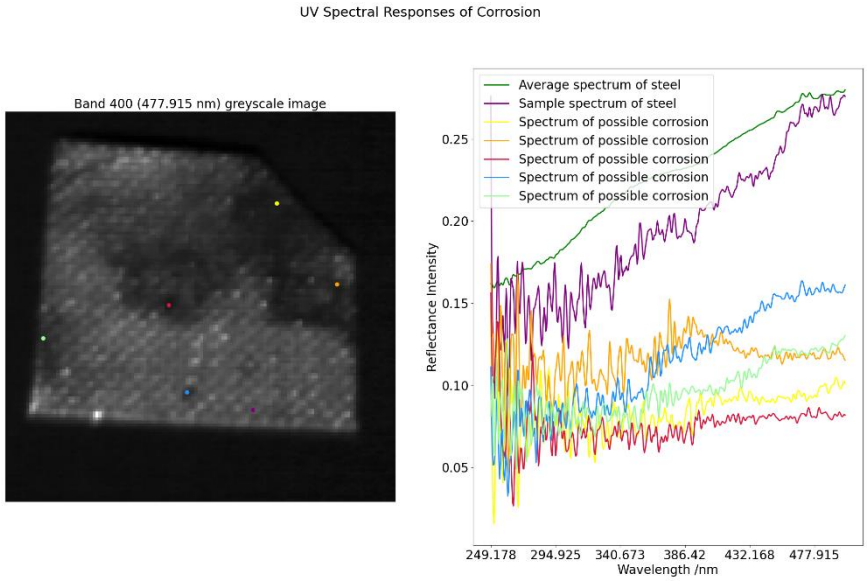

a) b)

Figure 5. a) Single UV band image of sample B with the pixels probed indicated on it; b) Probed UV corrosion spectra compared to the average and a sample 316L steel spectra

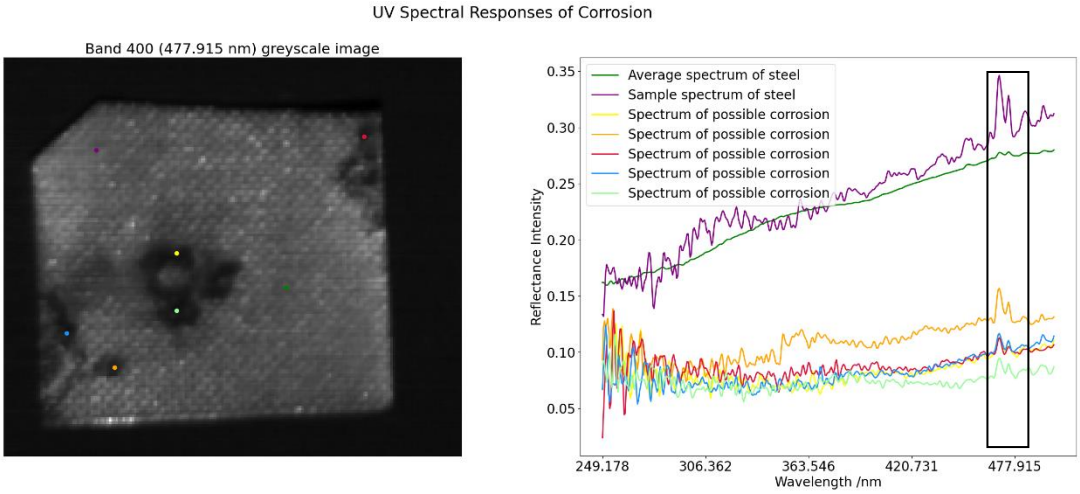

a) b)

Figure 6. a) Single UV band image of sample C with points probed indicated on it; b) Probed UV corrosion spectra compared to the average and a sample 316L steel spectra

The most reliable feature in separating the corrosion and steel spectra in the UV range is that the corrosion samples have lower general reflectivity than the steel. This is most apparent at higher wavelengths, heading towards the visible range.

1.2 VNIR Analysis (400 – 1000 nm)

The same corrosion and sample steel pixels on samples B and C were then probed in the VNIR range. Reviewing the spectra shows that areas of steel have a relatively flat spectral response. Areas of corrosion have a lower reflectivity between 400 – 500 nm, slowly rising to a peak and flattening off at around 700 nm. This S-

shaped curve can be reliably identified in all probed corroded areas in the VNIR for both samples B and C: Figure 7 and Figure 8.

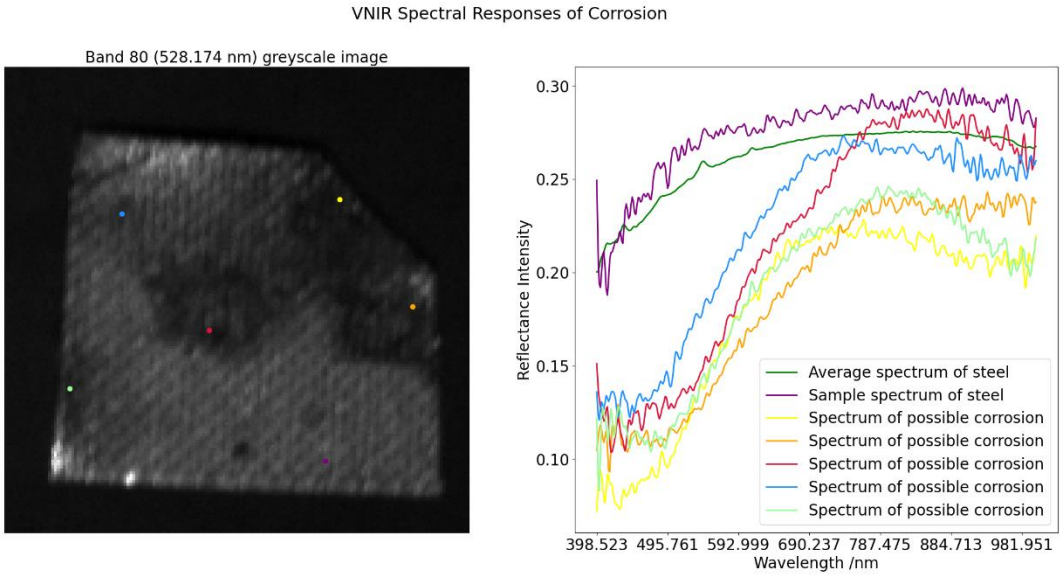

a) b)

Figure 7. a) Single VNIR band image of sample B with the pixels probed indicated on it; b) Probed VNIR corrosion spectra compared to the average and a sample 316L steel spectra

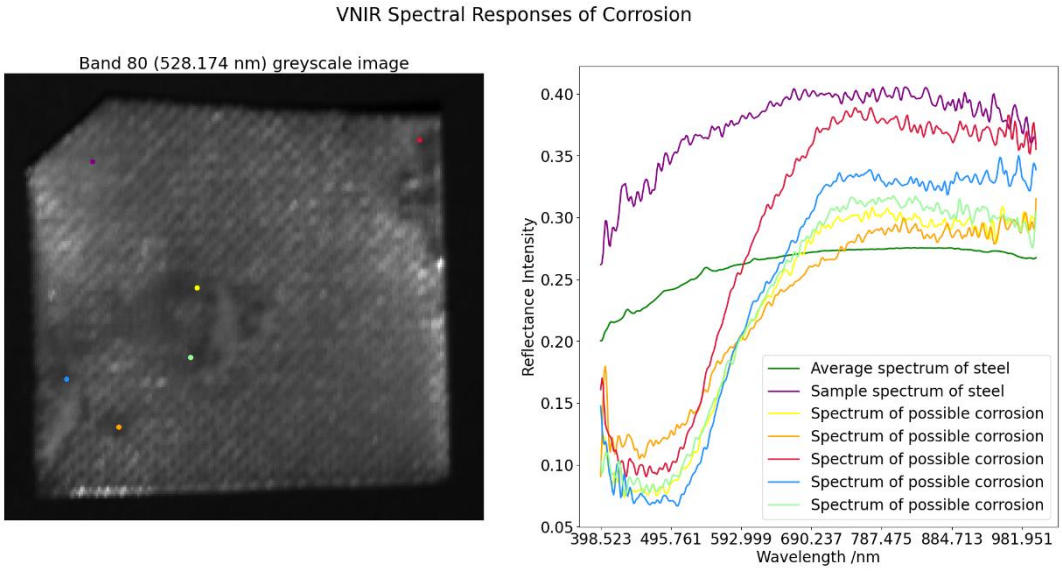

a) b)

Figure 8. a) Single VNIR band image of sample C with points probed indicated on it; b) Probed VNIR corrosion spectra compared to the average and a sample 316L steel spectra

1.3 SWIR Analysis (900 – 2500 nm)

Again, the same corrosion and steel pixels in samples B and C were assessed again for the SWIR wavelength range as seen in Figures 9 and 10, respectively. The SWIR spectra demonstrate strong spectral features, but lack the shared features amongst the corrosion points that were seen in the shorter wavelength ranges. For instance in

Figure 9b, the red spectrum has two peaks at around 1800 and 2100 nm; and in Figure 10b, the green and blue spectra share a dip at around 1900 nm.

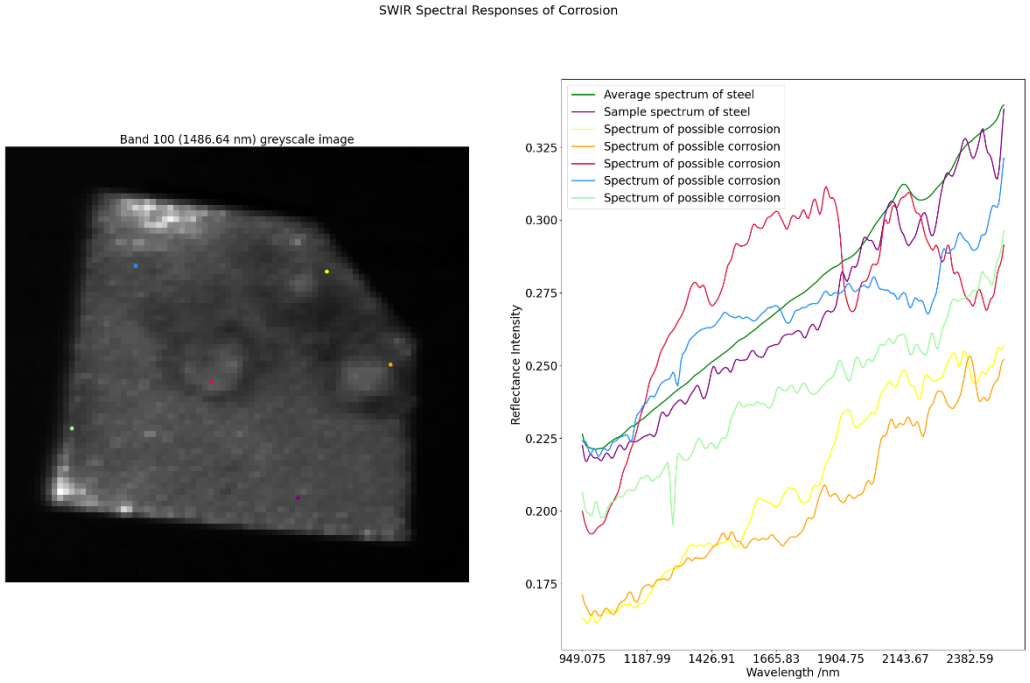

a) b)

Figure 9. a) Single band SWIR image of sample B with the pixels probed indicated on it; b) Probed SWIR corrosion spectra compared to the average and a sample 316L steel spectra

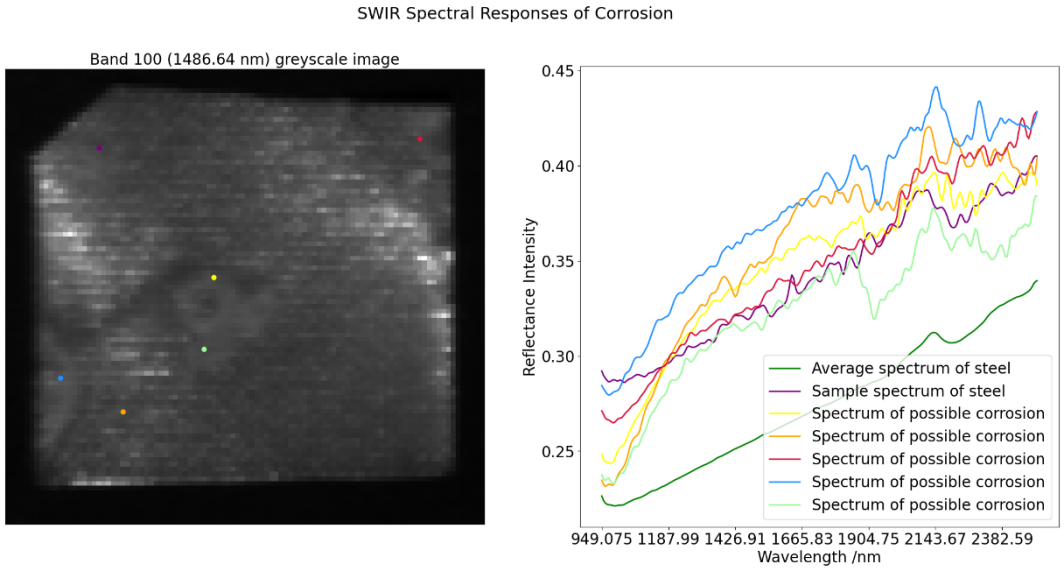

a) b)

Figure 10. a) Single band SWIR image of sample C with points probed indicated on it; b) Probed SWIR corrosion spectra compared to the average and a sample 316L steel spectra

5. DISCUSSION

Upon reviewing these initial results, the data indicate that, in the UV, corroded areas generally have lower reflectivity than that of pure 316L steel. The lower reflectivity of corroded steel relative to non-corroded steel may be attributed to a number of factors. For example, corroded surfaces are rougher than their steel counterparts, diffusing the reflected light such that only a fraction is sent back to the HSI camera. In the VNIR this same lower reflectivity can be identified for wavelengths between 400 - 500 nm, and the reflectivity increases between 600 – 700 nm. This is in line with what is expected of the rust-red hue of corrosion, and further supports the assertation made in [3]. The SWIR spectra examined did not share many features among corroded points, as determined by human visual inspection of the spectra. However, in literature, the SWIR spectral range was successfully exploited to identify different corrosion products on steel [4]. It is possible that the spectral features identified here may be indicative of different corrosion products, but missing the chemical characterisation of these samples, it is difficult to determine whether this is the case.

The double peaks that appear in the UV at 469 and 474 nm are not a reliable feature of corrosion, but as they appear on the corroded areas, further work is being done to determine whether they can be linked to a chemical characterisation. The wavelengths that these peaks occur at are also imageable by VNIR cameras, though analysis of the VNIR samples lit with the tungsten halogen light do not indicate that the peaks occur, and as such these features may be a function of the xenon illumination source. As such these peaks may be visible in data collected from the VNIR camera if paired with the xenon lamp.

Of the three ranges assessed, it appears that the VNIR range is the most effective range in separating steel and corrosion spectra. This is in line with the literature where hyperspectral VNIR spectra are commonly used in the identification of corrosion products in steel. The UV range also offers separable features and as such it may be worthwhile to consider this range when imaging steel to detect corrosion. The SWIR spectra exhibited many interesting features that are difficult to contextualise with only human visual inspection of the corroded areas.

6. CONCLUSIONS

This paper presents initial spectral results of corrosion on 316L steel using three hyperspectral imaging systems: the UV, VNIR, and SWIR wavelength ranges. These results support the literature that the VNIR range of spectra is highly informative in differentiating corrosion and steel. Extensive review of the literature available establishes that, to the best of the author's knowledge, this work is the first of its kind to analyse steel corrosion in UV range with a hyperspectral imaging system. These initial results have identified that in the UV range, corroded areas have lower reflectivity than that of non-corroded 316L steel. The results in the SWIR range assessed in this paper do not show conclusive features to separate the corrosion and steel spectra.

Further work will involve chemical assessment and identification of the corrosion products present on these samples to determine whether different corrosion products can be identified by unique spectral features in the 200 – 500 nm (UV), and whether the features found in the 900 – 2500 nm (SWIR) range are indicative of the presence of different iron oxides and hydroxides. Equally, this chemical assessment may give more context to the cause of the unexpected steel features in the UV range, namely the double peak at 469 and 474 nm. Further work will extend to examining these different spectra for features using machine learning techniques, supported by the chemical ground truth.

7. REFERENCES

[1] T. de Kerf, N. Hasheminejad, J. Blom, and S. Vanlanduit, "Qualitative Comparison of 2D and 3D Atmospheric Corrosion Detection Methods," Materials, vol. 14, no. 13, 2021, doi: 10.3390/ma14133621.

[2] Y. He, G. Tian, H. Zhang, M. Alamin, A. Simm, and P. Jackson, “Steel Corrosion Characterization Using Pulsed Eddy Current Systems,” IEEE Sens J, vol. 12, no. 6, pp. 2113–2120, 2012, doi: 10.1109/JSEN.2012.2184280.

[3] D. M. Sherman and T. D. Waite, “Electronic spectra of Fe3+ oxides and oxide hydroxides in the near IR to near UV.,” American Mineralogist, vol. 70, no. 11–12, pp. 1262–1269, 1985, [Online]. Available: http://pubs.er.usgs.gov/publication/70012311

[4] T. de Kerf, G. Pipintakos, Z. Zahiri, S. Vanlanduit, and P. Scheunders, “Identification of Corrosion Minerals Using Shortwave Infrared Hyperspectral Imaging,” Sensors (Basel), vol. 22, no. 1, Jan. 2022, doi: 10.3390/S22010407.

[5] D. N. Lavadiya, H. U. Sajid, R. K. Yellavajjala, and X. Sun, “Hyperspectral imaging for the elimination of visual ambiguity in corrosion detection and identification of corrosion sources:,” https://doi.org/10.1177/14759217211041690, vol. 0, no. 0, pp. 1–16, Aug. 2021, doi: 10.1177/14759217211041690.

[6] W. G. Rowley, “Hyperspectral Imaging for Detection of Corrosion on Intermediate Level Nuclear Waste Containers,” University of Birmingham, Birmingham, 2018. Accessed: May 31, 2022. [Online]. Available: https://etheses.bham.ac.uk//id/eprint/9070/1/Rowley2019PhD.pdf